Available online at www.sciencedirect.com
SCIENCE DIRECT
Journal of Sound and Vibration 295 (2006) 739–752
JOURNAL OF SOUND AND VIBRATION
www.elsevier.com/locate/jsvi

# Development of the numerical method for calculating sound radiation from a rotating dipole source in an opened thin duct

Han-Lim Choi*, Duck Joo Lee

*Division of Aerospace Engineering, Department of Mechanical Engineering, Korea Advanced Institute of Science and Technology, 373-1 Guseong-dong, Yuseong-gu, Daejeon 305-701, Republic of Korea*

Received 4 April 2005; received in revised form 8 December 2005; accepted 24 January 2006
Available online 17 April 2006

**Abstract**

Sound radiation from a rotating dipole source in an opened thin duct is analyzed using the thin-body boundary element method in the frequency domain. The difficulty in describing the rotating source in the frequency domain is overcome by introducing a fixed Kirchhoff surface around the rotating source. Acoustic pressures generated from a rotating dipole source, a rotating point force, on the Kirchhoff surface are calculated using Lowson's equation. Normal derivatives on the Kirchhoff surface of acoustic pressures in the Helmholtz integral equation are derived analytically in this paper. Radiated acoustic pressure from the Kirchhoff source and that of the rotating original source in a free field are compared. Effects of the number of elements on the Kirchhoff surface are verified. The analytic solution for a dipole source in a duct is compared with the one obtained by the current Kirchhoff–Helmholtz thin-body boundary element method (K–H TBEM). Sound radiation from a ducted rotating force is calculated using K–H TBEM for selected rotating speeds. It is shown that wave propagation is strongly dependent on the cutoff frequency of the duct. Radiated acoustic pressure can be increased or decreased according to the relation between the cutoff frequency of the duct and the rotating frequency of the source.


## 1. Introduction

There are many rotating systems in modern machinery. These systems create undesirable noise, which is generated by the fluctuation of the air around a rotating body. To solve this noise problem, many researchers have investigated sound generation from rotating sources. Lowson [1] first derived an equation for sound generation from rotating point forces in 1965. He considered a rotor to be a combination of point forces having lift terms and drag terms. Lowson's assumption was a good approximation of rotor noise source, because the major noise sources of a rotor are the pressures on the rotor blade.

In many cases, rotating sources are in a duct or in a case. The effects of the duct or the case cannot usually be included in either the Lowson equation or the Ffowcs Williams and Hawkings equation. Studies on sound radiation from rotating sources in a duct have focused on propagation and radiation for the last several decades. Tyler and Sofrin [2] first analyzed sound radiation of rotating sources in a duct using mode theories.

*Corresponding author. Tel.: +82 42 869 3756; fax: +82 42 869 3710.
*E-mail addresses:* airman10@kaist.ac.kr (H.-L. Choi), djlee@kaist.ac.kr (D.J. Lee).

0022-460X/$ - see front matter © 2006 Elsevier Ltd. All rights reserved.
doi:10.1016/j.jsv.2006.01.017

In their work, they considered a rotating fan as circumferentially distributed acoustic sources on a disk plane. Other researchers have studied duct propagation using finite element methods or boundary integral methods [3–5]. The majority of their work has been related to airplane turbo fan engines, which have many rotors and stators. These studies have enabled the analysis of sound radiation from rotating sources for realistic duct shapes. However, they have concentrated on propagation and radiation characteristics of the ducts rather than on the sources. They have generally considered rotating sources as a fixed source disk, on which various frequency components, measured or given, are distributed. This has been owing to the difficulty in describing rotating sources in the frequency domain used for the numerical method.

In recent years, a method has been developed that combines two fields, sound generation from a rotating source and radiation. Jeon and Lee [6] calculated the sound radiation from a centrifugal impeller near a wedge. They introduced a fixed Kirchhoff surface that enveloped the entire rotating source region, and the boundary element method (BEM) was used with the fixed Kirchhoff surface. They developed the Kirchhoff–Helmholtz boundary element method (K–H BEM) for a thick body to connect an impeller noise source to the BEM using the Kirchhoff surface, and they compared the numerical and experimental results. Jeon and Lee also applied the K–H BEM to a thin duct and obtained good results [7].

Although Jeon and Lee [7] applied successfully the Kirchhoff–Helmholtz thin body boundary element method (K–H TBEM) to actual ducted fan systems, all processes of the method were not sufficiently verified, particularly for the normal derivative of the acoustic pressures from the rotating sources in the Helmholtz integral method, an important term in K–H TBEM. In this paper, normal derivatives of acoustic pressures from rotating sources are derived analytically, and all processes of the method are verified in several examples. The newly derived method is applied to the analysis of sound radiation from rotating sources in an opened thin duct.

## 2. Procedure for numerical implementation

Analyses of sound fields generated by a rotating source in an opened thin duct cannot be obtained using the conventional method. Therefore, the Kirchhoff–Helmholtz boundary integral equation (K–H BIE) was introduced by Jeon and Lee [6]. There are three steps to formulate the K–H BIE. The first step is to calculate the sound fields generated by the rotating source. The second step is to model the source using the fixed Kirchhoff source. The final step is to analyze acoustic scattering by a thin body. Fig. 1 shows a schematic diagram of the entire process. The sound generated from a rotating source is calculated using Lowson's equation. The sound obtained using Lowson's equation is expressed as time varying pressure signals. To apply a pressure signal $p(t)$ to the frequency domain boundary integral equation as an input source, $p(t)$ should be transformed into $p(\omega)$. This is the second step using the Kirchhoff source. If the fixed Kirchhoff source is obtained from the rotating sources, it can be substituted perfectly for the original source. Acoustic scattering by a body can be calculated by solving the boundary integral equation, because the acoustic pressures at any

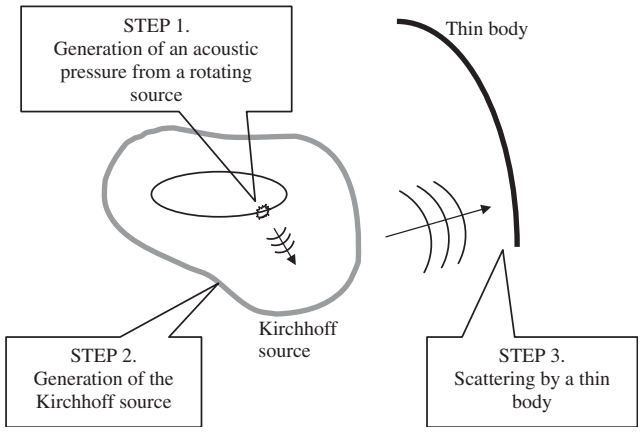


Fig. 1. A schematic diagram of the three steps of the K–H BEM for a thin body.

points out of the Kirchhoff source can be easily obtained by integrating the sources on the Kirchhoff surface. Details of the K–H BEM are thoroughly explained by Jeon and Lee [6]. In this paper, the K–H BEM for a thin body is refined and validated, particularly with regard to the modeling of the Kirchhoff source.

### 2.1. Acoustic field of rotating point forces

Several methods can be used for calculating the acoustic field of rotating sources. A dipole term is used in this paper to represent the noise from the rotating force. Lowson's equation for the dipole can be written as follows [1]:

$$4\pi p(\mathbf{x}, t) = \left[\frac{1}{a_0 r(1-M_r)^2}\left(\dot{F}_r + \frac{F_r \dot{M}_r}{(1-M_r)}\right) + \frac{1}{r^2(1-M_r)^2}\left(F_r\frac{(1-M^2)}{(1-M_r)} - F_i M_i\right)\right], \quad (1)$$

where $p$ is the acoustic pressure, $F$ is the rotating force vector, $a_0$ is the speed of sound and $i$ is the tensor index. The square brackets denote that the functions inside the bracket should be evaluated at the retarded time $\tau = t - r/a_0$. Where $\tau$ is the time of observation and $r$ is the distance from source to observer. Fig. 2 shows a rotating point force and some vector notations, as follows: $\mathbf{r}$ is the vector from a source to an observer; $\boldsymbol{\omega}$ is the angular velocity vector of a rotating force and $\mathbf{M} = \boldsymbol{\omega} \times \mathbf{y}/a_0$; and $\mathbf{x}$ and $\mathbf{y}$ are the position vectors of an observer and a source, respectively. $M_r$ and $F_r$ are defined as $F_r = (x_i - y_i)F_i/r$ and $M_r = (x_i - y_i)M_i/r$. The first and second terms of right-hand side of Eq. (1) represent the sound pressure owing to the time variation of an unsteady force and the acceleration of the source.

### 2.2. The Kirchhoff source and its analytic generation

#### 2.2.1. The Kirchhoff source

In general, rotor systems and fan systems have scattering objects such as ducts or helicopter bodies. In that case, the scattered acoustic field in the frequency domain is usually solved by the BEM. This scattering analysis requires a stationary source to represent rotating sources as input sources conveniently; the K–H BEM was developed to meet this requirement [6]. The key idea of the K–H BEM is the use of the Kirchhoff source modeling of the original rotating sources. The Kirchhoff source is usually represented as a closed surface called the Kirchhoff surface. The Kirchhoff surface is a virtual surface that encloses all rotating sources, as shown in Fig. 3. The Kirchhoff surface contains all the information of the acoustic sources. The characteristics of various acoustic sources are replaced by pressure and its derivative on the Kirchhoff surface. Because the usual BEM requires a frequency domain source, time domain pressures and their derivatives on the Kirchhoff source are transformed into frequency domain data. Pressure at an observer position $P$ can be calculated by

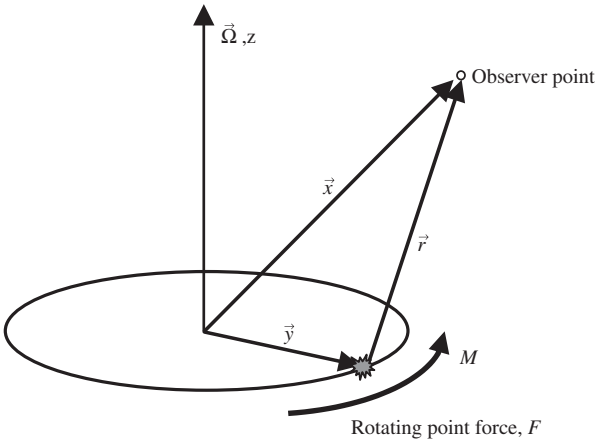


Fig. 2. A rotating point force and related variables.

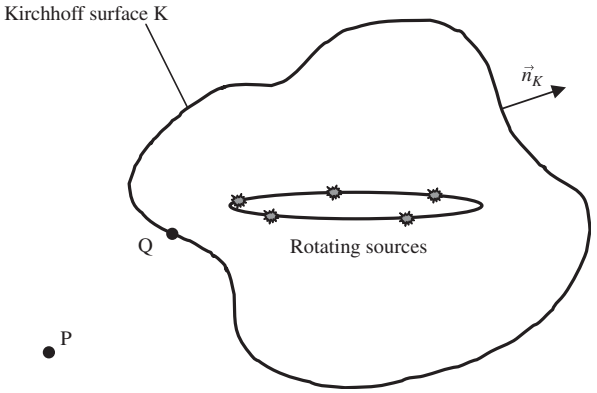


Fig. 3. A schematic diagram of rotating sources enclosed by the Kirchhoff surface.

the surface integration on the Kirchhoff surface, as follows:

$$p(P) = \frac{1}{4\pi}\int_K \left\{ p(Q)\frac{\partial G}{\partial n_K}(P,Q) - \frac{\partial p}{\partial n_K}(Q)G(P,Q)\right\} \mathrm{d}K(Q), \tag{2}$$

where $p(P)$ is the acoustic pressure at $P \notin K$, $K$ is the Kirchhoff surface, $Q \in K$ is a source position on $K$, $p(Q)$ and $\partial p/\partial n_K(Q)$ are pressure and its normal derivative, respectively, on the Kirchhoff surface $K$. $G(P,Q)$ and $\partial G/\partial n_K(P,Q)$ are the free field Green function and its normal derivative, respectively, on the surface. While the shape of the Kirchhoff surface can be arbitrary in general, the cylindrical Kirchhoff surface is selected for its convenient application to the rotating sources.

*2.2.2. Derivation of the analytic Kirchhoff source*

Two important variables, $p(Q)$ and $\partial p/\partial n_K(Q)$, should be obtained from the original sources using Eq. (1). Jeon and Lee [6] generated three independent Kirchhoff surfaces for obtaining these variables, as shown in Fig. 4. One Kirchhoff surface is used for obtaining $p(Q)$ and two other Kirchhoff surfaces are used for obtaining $\partial p/\partial n_K(Q)$ numerically. While it is easy to obtain the necessary variables with this method, it takes time to generate the three Kirchhoff sources. The source generation step on the Kirchhoff source from the rotating sources takes nearly the entire process time for calculating the sound radiation of the rotating sources, including scattering. Another disadvantage of using the numerical methods of Jeon and Lee to obtain $\partial p/\partial n_K(Q)$ is the accuracy of the Kirchhoff surface. For sufficient accuracy when using the numerical method, the size of $\Delta \mathbf{n}_K$ should be in the range where acoustic pressures vary linearly.

In this paper, $\partial p/\partial n_K(Q)$ is obtained analytically for more elaborate and faster generation of the Kirchhoff surface. The tensor form of Eq. (1) can be written as follows:

$$p = \frac{1}{4\pi[1-M_r]}\left\{ [F_i]\frac{\partial}{\partial y_i}\left[\frac{1}{r}\right] + \left[\frac{(x_i-y_i)}{a_0 r^2}\frac{\partial F_i}{\partial t}\right] + \frac{\partial}{\partial y_i}\left[\frac{(x_i-y_i)F_i M_i}{r^2(1-M_r)}\right]\right\}. \tag{3}$$

Again, the square brackets denote that the functions inside the bracket should be evaluated at the retarded time $\tau = t - r/a_0$. If Eq. (3) is differentiated with an unit vector $\mathbf{n}_K$ on the Kirchhoff surface,

$$\begin{aligned}
\frac{\partial p}{\partial \mathbf{n}_K} &= \left(\frac{\partial p}{\partial x_1}, \frac{\partial p}{\partial x_2}, \frac{\partial p}{\partial x_3}\right)\cdot \mathbf{n}_K = \frac{\partial p}{\partial x_j} n_{Kj},\\
\frac{\partial p}{\partial x_j} &= \frac{\partial}{\partial x_j}\left(\frac{1}{4\pi[1-M_r]}\left\{ [F_i]\frac{\partial}{\partial y_i}\left[\frac{1}{r}\right] + \left[\frac{(x_i-y_i)}{a_0 r^2}\frac{\partial F_i}{\partial t}\right] + \frac{\partial}{\partial y_i}\left[\frac{(x_i-y_i)F_i M_i}{r^2(1-M_r)}\right]\right\}\right),
\end{aligned} \tag{4}$$

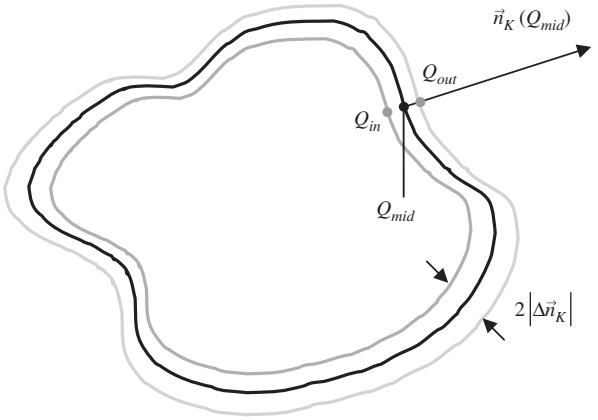


Fig. 4. Numerical calculation of $p(Q)$ and $\partial p/\partial n_K(Q)(Q_{\text{mid}} \in K_{\text{mid}}, Q_{\text{in}} \in K_{\text{in}}, Q_{\text{out}} \in K_{\text{out}})$.

where $p(\mathbf{x}, t) = f\left(\mathbf{x}, \mathbf{y}(t - r/a_0)\right)$, $r = \sqrt{(x_1 - y_1(\tau))^2 + (x_2 - y_2(\tau))^2 + (x_3 - y_3(\tau))^2}$ and $\tau = t - r/a_0$. $\partial r/\partial x_j$ is obtained as below:

$$\frac{\partial r}{\partial x_j} = \frac{\hat{r}_j}{1 - M_r}, \tag{5}$$

where $M_r = (x_i - y_i)M_i/r$.

The final analytic form of $\partial p/\partial \mathbf{n}_K$ is

$$\begin{aligned}\frac{\partial p}{\partial \mathbf{n}_K} = \frac{\partial p}{\partial x_j} n_{Kj} = \frac{1}{4\pi c}\left[\left(\dot{F}_r + \frac{F_r \dot{M}_r}{1 - M_r}\right)A + \frac{1}{r(1 - M_r)^2}B\right]n_{Kj} \\ + \frac{1}{4\pi}\left[\left(F_r \frac{1 - M^2}{1 - M_r} - F_i M_i\right)C + \frac{1}{r^2(1 - M_r)^2}D\right]n_{Kj},\end{aligned} \tag{6}$$

where

$$\begin{aligned}A &= -\frac{\partial r}{\partial x_j}\frac{1}{r^2(1 - M_r)^2} + \frac{2}{r(1 - M_r)^3}\frac{\partial M_r}{\partial x_j}, \\ B &= \frac{\partial \dot{F}_r}{\partial x_j} + \frac{1}{1 - M_r}\left(\dot{M}_r \frac{\partial F_r}{\partial x_j} + F_r \frac{\partial \dot{M}_r}{\partial x_j}\right) + \frac{F_r \dot{M}_r}{(1 - M_r)^2}\frac{\partial M_r}{\partial x_j}, \\ C &= -\frac{2}{r^3(1 - M_r)^2}\frac{\partial r}{\partial x_j} + \frac{2}{r^2(1 - M_r)^3}\frac{\partial M_r}{\partial x_j}, \\ D &= \frac{1 - M^2}{1 - M_r}\frac{\partial F_r}{\partial x_j} + \frac{1 - M^2}{(1 - M_r)^2}\frac{\partial M_r}{\partial x_j} \\ &\quad - \left(\frac{\partial F_1}{\partial x_j}M_1 + \frac{\partial M_1}{\partial x_j}F_1 + \frac{\partial F_2}{\partial x_j}M_2 + \frac{\partial M_2}{\partial x_j}F_2 + \frac{\partial F_3}{\partial x_j}M_3 + \frac{\partial M_3}{\partial x_j}F_3\right).\end{aligned} \tag{7}$$

### 2.3. Acoustic scattering by a thin body with the Kirchhoff source

#### 2.3.1. Acoustic scattering by a thin body

In this paper, to calculate the acoustic scattering by a thin body the direct thin body boundary element method is used [8,9]. This direct method has some advantages over the indirect method or multi-domain method in terms of calculation time and the ease of imposing boundary conditions. Fig. 5 shows a schematic diagram of acoustic scattering by a thin body and notations of some variables. As derived in the paper of Wu

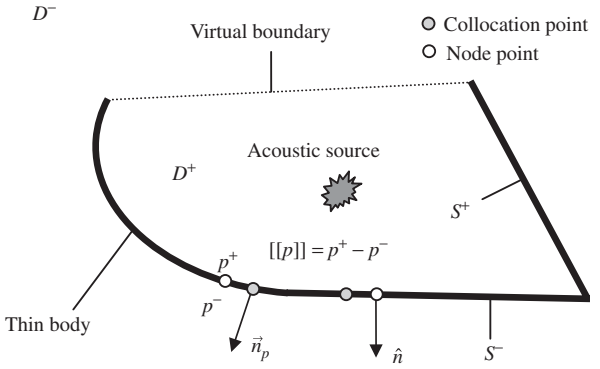


Fig. 5. A schematic diagram of acoustic scattering by a thin body.

and Wan [8], the normal derivative Helmholtz integral equation is written as

$$\int_S \{(\hat{n}_p \times \nabla_p G) \cdot (\hat{n} \times \nabla[[p]]) + k^2(\hat{n}_p \cdot \hat{n})G[[p]]\}\, \mathrm{d}S = 4\pi \frac{\partial p}{\partial n_p} + 4\pi \frac{\partial p_{\text{source}}}{\partial n_p}. \tag{8}$$

We use $p$ as a variable instead of velocity potential $\phi$ in Ref. [8] and $p = -\rho\partial\phi/\partial t$. The term $\hat{n}_p$ is a normal vector at a collocation point on a body surface $S$; $\mathbf{n}$ is a normal vector at a node point on $S$; $[[p]] = p^+ - p^-$; $p^+$ and $p^-$ are pressures on $S^+$ and $S^-$, respectively. The term $k$ is a wavenumber, and $p_{\text{source}}$ is the pressure of the incident wave reached on a surface $S$ from the acoustic sources. Unknowns in Eq. (10) are acoustic pressure difference across the thin body, $[[p]]$, as shown in Fig. 5. $[[p]]$ can be obtained using the surface boundary condition $\partial p/\partial n_p$ and the incident wave term $\partial p_{\text{source}}/\partial n_p$. Detailed formulations and solution methods are shown by Wu and Wan for a rigid body [8] and by Ih and Lee for a body having general boundary conditions [9].

### 2.3.2. K–H TBEM—application of the Kirchhoff source to the normal derivative Helmholtz integral equation for a thin body

To obtain the scattered acoustic pressure fields owing to a thin body, the source term should be represented as the form of normal derivatives of source pressures, as shown on the right-hand side of Eq. (10), $\partial p_{\text{source}}/\partial n_p$. Because the source term in Eq. (10) is the form of $\partial p_{\text{source}}/\partial n_p$ not $p_{\text{source}}$, the normal derivative of pressure in Eq. (2) is obtained as below

$$\begin{aligned}\frac{\partial p_{\text{source}}(P)}{\partial n_p} &= \frac{1}{4\pi}\frac{\partial}{\partial n_p}\int_K \left\{ p(Q)\frac{\partial G}{\partial n_K}(P,Q) - \frac{\partial p}{\partial n_K}(Q)G(P,Q)\right\} \mathrm{d}K(Q) \\ &= \frac{1}{4\pi}\int_K \left\{ p(Q)\frac{\partial^2 G}{\partial n_p \partial n_K}(P,Q) - \frac{\partial p}{\partial n_K}(Q)\frac{\partial G}{\partial n_p}(P,Q)\right\} \mathrm{d}K(Q),\end{aligned} \tag{9}$$

where $p(P)$ is the acoustic pressure at $P \notin K$, $K$ is the Kirchhoff surface, $Q \in K$ is a source position on $K$, $p(Q)$ and $\partial p/\partial n_K(Q)$ are the pressure and its normal derivative, respectively, on the Kirchhoff surface $K$, as explained in Section 2.2.1. $G(P,Q)$ and $\partial G/\partial n_K(P,Q)$ are the free field Green function and its normal derivative, respectively. Because $p(Q)$ and $\partial p/\partial n_K(Q)$ are obtained from a known rotating source, all terms on the right-hand side of Eq. (11) are known. Accordingly, $\partial p_{\text{source}}(P)/\partial n_p$ is also known. If $\partial p_{source}/\partial n_p$ on the right-hand side of Eq. (10) is replaced by Eq. (11), sound scattering from the Kirchhoff source owing to a thin body can be analyzed. $p(Q)$ and $\partial p/\partial n_K(Q)$ in Eq. (11) are obtained using Eqs. (3) and (8).

$\partial^2 G/\partial n_p \partial n_K$ in Eq. (11) can be expanded as below

$$\frac{\partial^2 G}{\partial n_p \partial n_K} = \nabla_p \left(\frac{\partial G}{\partial n_K}\right) \cdot \mathbf{n}_p,$$
$$\nabla_p \left(\frac{\partial G}{\partial n_K}\right) = -\nabla_p \left(jk + \frac{1}{r}\right) G \frac{\partial r}{\partial n_K} - \nabla_p (G) \left(jk + \frac{1}{r}\right) \frac{\partial r}{\partial n_K} - \nabla_p \left(\frac{\partial r}{\partial n_K}\right) G \left(jk + \frac{1}{r}\right), \tag{10}$$

where

$$\frac{\partial G}{\partial n_K} = -\left(jk + \frac{1}{r}\right) G \frac{\partial r}{\partial n_K}. \tag{11}$$

The final form of Eq. (12) should be written as

$$\frac{\partial^2 G}{\partial n_p \partial n_K} = \nabla_p \left(\frac{\partial G}{\partial n_K}\right) \cdot \mathbf{n}_p = (A + B + C) \cdot \mathbf{n}_p, \tag{12}$$

where

$$A = \frac{1}{r^2} G \frac{\partial r}{\partial n_K} \left(\frac{x_1 - y_1}{r}, \frac{x_2 - y_2}{r}, \frac{x_3 - y_3}{r}\right),$$
$$B = \left(-k^2 + \frac{2kj}{r} + \frac{1}{r^2}\right) G \frac{\partial r}{\partial n_K} \left(\frac{x_1 - y_1}{r}, \frac{x_2 - y_2}{r}, \frac{x_3 - y_3}{r}\right),$$
$$C = \frac{G}{r} \left(jk + \frac{1}{r}\right) \left(n_{K1} + \frac{\partial r}{\partial n_K} \frac{\partial r}{\partial x_1}, n_{K2} + \frac{\partial r}{\partial n_K} \frac{\partial r}{\partial x_2}, n_{K3} + \frac{\partial r}{\partial n_K} \frac{\partial r}{\partial x_3}\right),$$
$$\mathbf{n}_K = n_{K1} \hat{i} + n_{K2} \hat{j} + n_{K3} \hat{k}. \tag{13}$$

## 3. Validations of methods and numerical results

### 3.1. Acoustic pressures of a rotating dipole source in a free field

Fig. 6 shows nondimensionalized acoustic pressures in the time domain and their spectrums for a rotating dipole source at a selected observer angle $\theta = 0^\circ$, $30^\circ$, $60^\circ$, $80^\circ$, $90^\circ$. The diameter of the source is $D_s$, the angular velocity of the source is $\Omega$ and the source rotates at nondimensionalized speed $v^* = D_s\Omega/2a_0 = 0.00294\pi$. The observer distance $r$ is $1.0D_s$. In Fig. 6, acoustic pressures in time domain and sound pressure level in frequency domain are shown for a rotating source having a lift force only, $F = F_3$ in Eq. (1), $f$ is the frequency. The pressure, time and frequency are nondimensionalized as $p^* = pD_s^2/|F|$, $t^* = \Omega t/2\pi$ and $f^* = 2\pi f/\Omega$. The nondimensionalized blade passage frequencies (BPFs) of the source are $f^* = 1, 2, 3 \ldots$ . As $\theta$ decreases, the shape of the acoustic pressures becomes sharper. Consequently, higher harmonics appear noticeably for lower angles in Fig. 6. In other words, the contributions of higher harmonics from the rotating dipole source decrease for higher values of $\theta$. Fig. 7 shows directivity patterns of the nondimensionalized acoustic pressure, $p^*$, from the rotating source in a free field. Most of the sound radiates for $\theta = 30^\circ - 60^\circ$ and no sound radiates for $\theta = 0^\circ$ or $90^\circ$.

### 3.2. Validation of the Kirchhoff source

Two major factors should be satisfied so that the Kirchhoff source can be a good model of a rotating source. The first factor is the accuracy of the variables $p_K$ and $\partial p/\partial \mathbf{n}_K$ on the Kirchhoff surface. The second factor is the accuracy of the acoustic pressure and its derivative (Eqs. (2) and (11)) at an observer point, such as on the thin body. Both factors of the Kirchhoff source are tested in this paper.

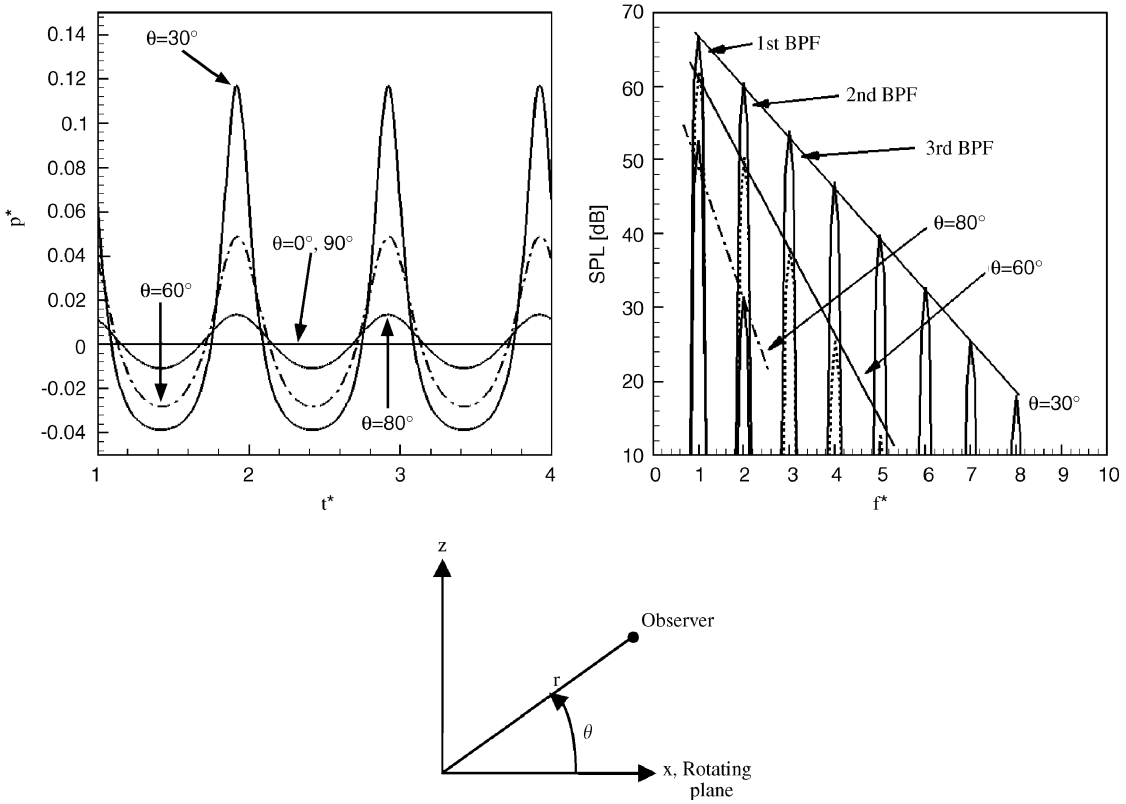


Fig. 6. Nondimensionalized acoustic pressures and spectrums of a rotating dipole source in a free field at $r = 1.0D_s$ ($p^* = pD_s^2/|F|$, $t^* = \Omega t/2\pi$ and $f^* = 2\pi f/\Omega$).

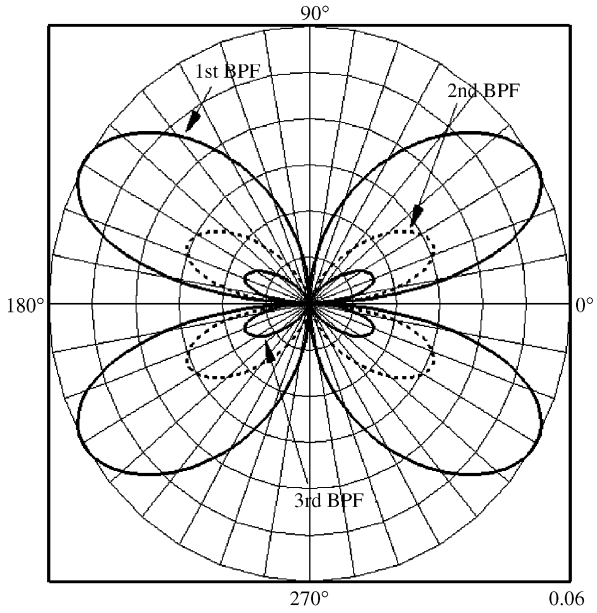


Fig. 7. Nondimensionalized acoustic directivity patterns from a rotating dipole source in a free field at $r = 1.0D_s$ $\left(p^* = pD_s^2/|F|\right)$.

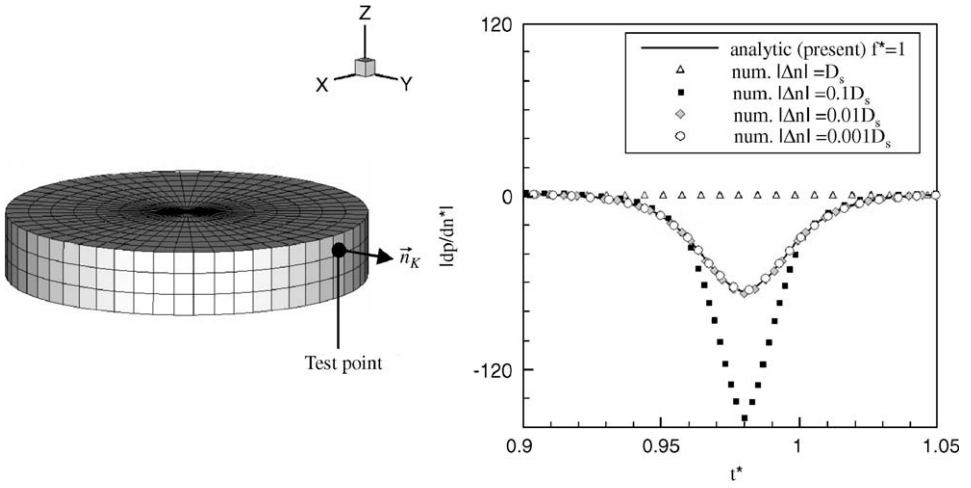


Fig. 8. Comparisons of numerical $|\partial p^*/\partial \mathbf{n}_K|$ in the time domain with analytic $|\partial p^*/\partial \mathbf{n}_K|$ at the test point on the Kirchhoff surface $(|\partial p^*/\partial \mathbf{n}_K| = |\partial p/\partial \mathbf{n}_K/D_s^3|)$.

### 3.2.1. *Accuracy of the surface variable $\partial p/\partial \mathbf{n}_K$ on the Kirchhoff surface*

To check the accuracy of the numerical representation of $\partial p/\partial \mathbf{n}_K$ on the Kirchhoff surface $K$, the numerically obtained $\partial p/\partial \mathbf{n}_K$ is compared with the present $\partial p/\partial \mathbf{n}_K$ obtained by analytic formulation (Eq. (8)) at a selected point on the Kirchhoff surface $K$ with a variable $|\Delta \mathbf{n}|$. The tested dipole source represents lift force only, $F = F_3$ and it rotates in the $xy$ plane with a diameter $D_s$. Fig. 8 shows comparisons of the numerical nondimensionalized $|\partial p/\partial \mathbf{n}_K|$, $|\partial p^*/\partial \mathbf{n}_K|$, in the time domain with the analytic $|\partial p^*/\partial \mathbf{n}_K|$. The normal derivative of the pressure is nondimensionalized as $|\partial p^*/\partial \mathbf{n}_K| = \partial p/\partial \mathbf{n}_K/D_s^3$. It is shown that the accuracy of the numerical results highly depends on the magnitude of $|\Delta \mathbf{n}|$. Furthermore, as stated earlier, the numerically obtained Kirchhoff source requires a much longer calculation time than the present analytic Kirchhoff source and most of computing time is used for the calculation of the Kirchhoff sources.

### 3.2.2. *Accuracy of the acoustic pressure and its normal derivative on the duct*

Fig. 9 shows a comparison of the exact values of $|p^*|$ and $|\partial p^*/\partial n_p|$ in Eqs. (3) and (6) with values obtained using the Kirchhoff surface at the observer points on the duct wall. The diameter of the duct is $20D_s$ and the diameter of the cylindrical Kirchhoff surface is $1.2D_s$. Because the accuracy of the Kirchhoff source is affected by both the number of elements and the source frequencies, the Kirchhoff source is tested for several element numbers and several BPFs of the source. The tested rotating speed is $v^* = 0.0147\pi$. The BPFs of the source are $f^* = 1, 2, 3 \ldots$ . For a small number of elements, the Kirchhoff source cannot represent acoustic pressures and their normal derivatives from the original source. As the number of elements on the source increases and the calculated frequency decreases, the discrepancy between the two sets of data decreases. It is shown that the Kirchhoff source can substitute for the original rotating sources very well.

### 3.2.3. *Validation of K–H TBEM*

Sound radiation from a ducted stationary dipole in a thin opened duct is analyzed by the K–H TBEM because analytic solutions exist. Fig. 10 shows a schematic diagram of the problem, a far-field acoustic directivity of a ducted stationary dipole, which is modeled as the Kirchhoff source. Detailed geometries of the problem are shown in the paper of Martinez [10]. In Fig. 10, the acoustic directivities using K–H TBEM is compared with the analytic ones [10]. The results of the proposed K–H TBEM with 64 duct elements show good agreements with the analytic ones. Although the modeled source is a stationary dipole not a rotating dipole, it is enough to validate the K–H TBEM because the source modeling procedure using the Kirchhoff source is the same for the stationary source and the rotating source.

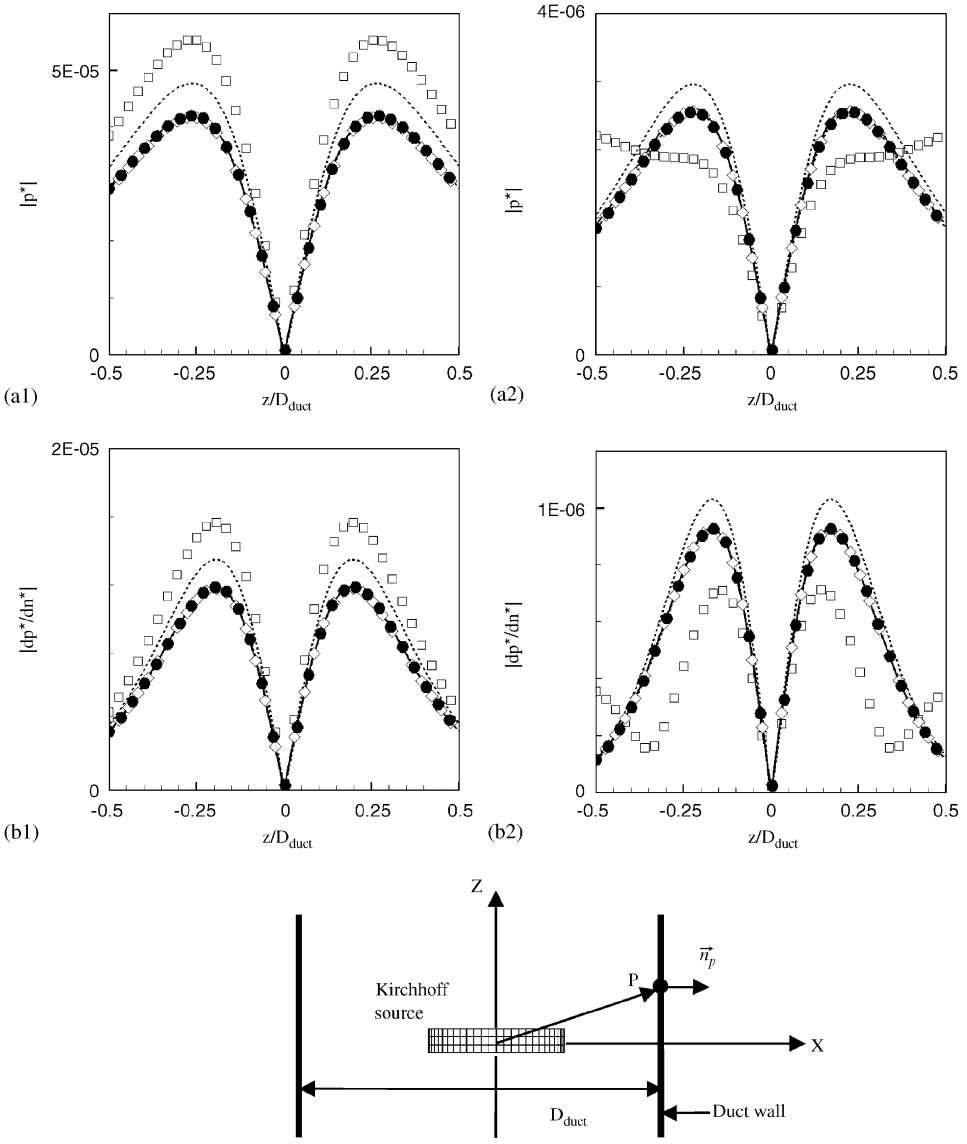


Fig. 9. Effect of the Kirchhoff element on $|p^*|$ and $|\partial p^*/\partial \mathbf{n}_p|$ at $P$ on the duct wall at $v^* = 0.0147\pi$ (——: analytic, □: 82 Kirchhoff elem., - - - -: 254 Kirchhoff elem., ◇: 434 Kirchhoff elem., ●: 1066 Kirchhoff elem., (a1): $|p^*|$—the 1st BPF, (a2): $|p^*|$—the 2nd BPF, (b1): $|\partial p^*/\partial n|$—the 1st BPF, (b2): $|\partial p^*/\partial n|$—the 2nd BPF).

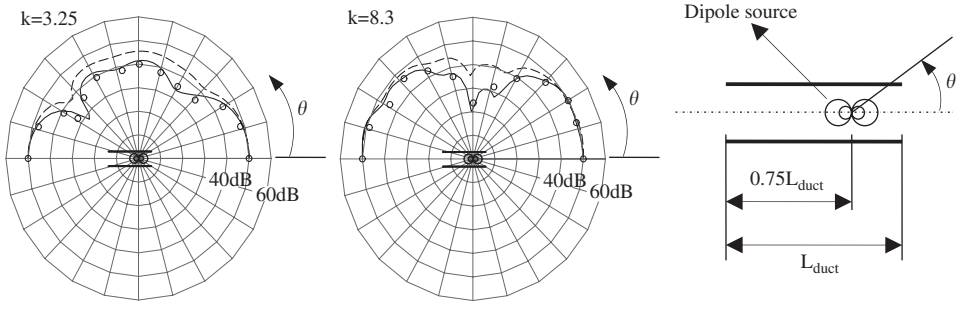


Fig. 10. Effect of the duct element on the acoustic radiation of a ducted dipole (- - - -: K–H TBEM (32 duct elements), ——: K–H TBEM (64 duct elements), ○: Martinez).

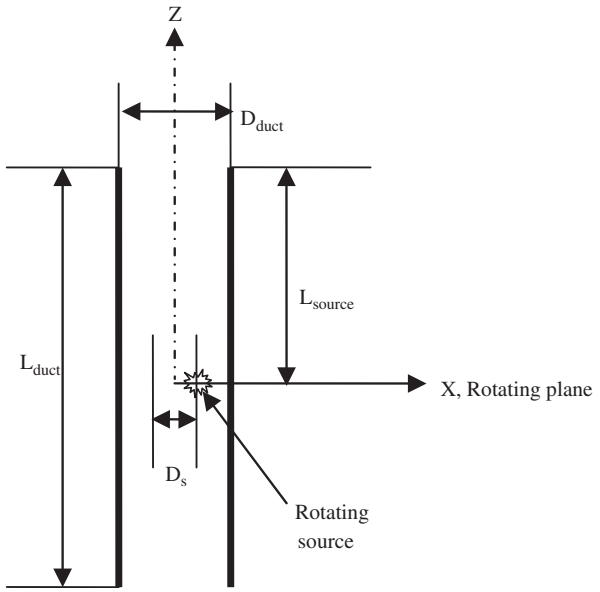


Fig. 11. A schematic diagram of a ducted rotating source and definitions of axes ($L_{\text{duct}} = 5.0D_{\text{duct}}$, $L_{\text{source}} = 2.5D_{\text{duct}}$), $D_{\text{duct}} = 20D_s$).

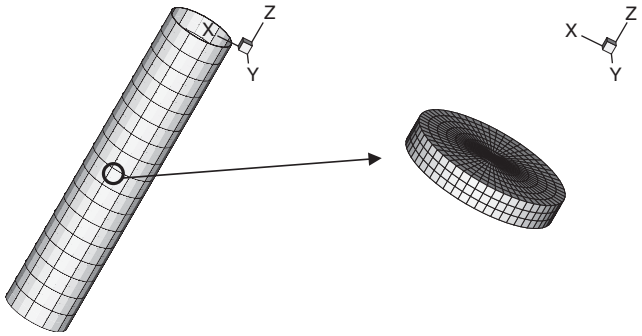


Fig. 12. Calculating meshes on a duct and the Kirchhoff source.

### 3.3. Sound radiation from a rotating source in a circular duct with the K–H TBEM

Generally, an acoustic source in a duct can be thought as the combination of infinite number of duct modes. Some sources are composed of a few modes and some are composed of many duct modes. In these cases, some modes can propagate through a duct and some modes cannot. These propagation phenomena are determined by the geometry of the duct. Among these modes, a plane wave mode can always propagate without exponential decay for rigid ducts. However, if the source does not have a plane wave mode and only have other higher modes, it can be decayed exponentially even for a rigid duct case. Because each BPF of the rotating dipole source considered in this paper has little plane wave mode and has a specific rotating mode, some can be diminished in spite of a rigid duct.

Acoustic fields of a ducted rotating dipole source are analyzed with the proposed K–H TBEM. Fig. 11 shows a schematic diagram of a ducted rotating source and Fig. 12 shows numerical meshes on the Kirchhoff source and on the circular duct. All surfaces of the infinitesimally thin duct used for calculation are rigid, $\partial p/\partial n = 0$ on duct surfaces. The diameter of the duct, $D_{\text{duct}}$, is $20D_s$. The diameter and the height of the cylindrical Kirchhoff surface are $1.2D_s$ and $0.4D_s$, respectively.

### 3.3.1. Cutoff frequency in the duct

Fig. 13 shows instantaneous nondimensionalized acoustic pressure contours of the rotating dipole source in a free field and in the duct. (a1), (a2) and (a3) are the instantaneous nondimensionalized acoustic pressure contours of the rotating source in a free field. The nondimensionalized rotating speed of the source is $0.0265\pi$. The first BPF of the rotating source, $f^*$, is 1. The patterns of radiation are similar when the source is in a free field. However, if the source rotates in a duct, the acoustic fields are completely different (see (b1), (b2) and (b3)). For the case of the first BPF, it is cutoff (see Table 1) and acoustic waves exponentially decay through the duct (see (b1)). The magnitude of the radiated sound for the first BPF is much smaller than that for the free field case (see (a1)). On the other hand, acoustic waves regularly propagate and radiate for the second and third BPF cases, because they are cuton (see Table 1). The acoustic fields of the source in a duct (see (b2) and (b3)) become more complex than those of the source in a free field (see (a2) and (a3)) owing to diffraction at both edges of the duct.

### 3.3.2. Directivity patterns

Fig. 14 shows directivity patterns of the nondimensionalized acoustic pressures, $p^*$, from the rotating source in a free field and in the duct at $r = 7.5D_{\text{duct}}$. The magnitude of (a1), (a2) and (a3) in Fig. 14 is 10 times the

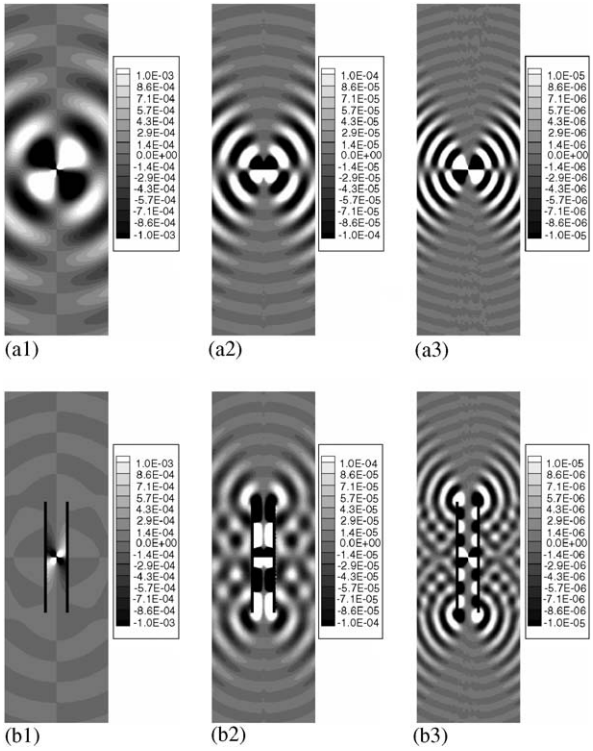


Fig. 13. Instantaneous nondimensionalized acoustic pressure contours of a rotating dipole source, at $v^* = 0.0265\pi$ ((a1): free field—the 1st BPF, (a2): free field—the 2nd BPF, (a3): free field—the 3rd BPF, (b1): ducted field—the 1st BPF (cutoff), (b2): ducted field—the 2nd BPF (cuton), (b3): ducted field—the 3rd BPF (cuton), $v^* = D_s\Omega/2a_0$).

Table 1
Cutoff frequencies of a circular duct ($D_{\text{duct}} = 20D_s$, radial mode = 1) and rotating frequencies of a rotating source

| BPF | $f^*(v^* = 0.0265\pi)$ | Circumferential mode, $m = 1$ $(f^*_{\text{cutoff}} = 1.1067)$ | Circumferential mode, $m = 2$ $(f^*_{\text{cutoff}} = 1.8333)$ | Circumferential mode, $m = 3$ $(f^*_{\text{cutoff}} = 2.5256)$ |
|---|---|---|---|---|
| 1st | 1 | Cutoff | Cutoff | Cutoff |
| 2nd | 2 | Cuton | Cuton | Cutoff |
| 3rd | 3 | Cuton | Cuton | Cuton |

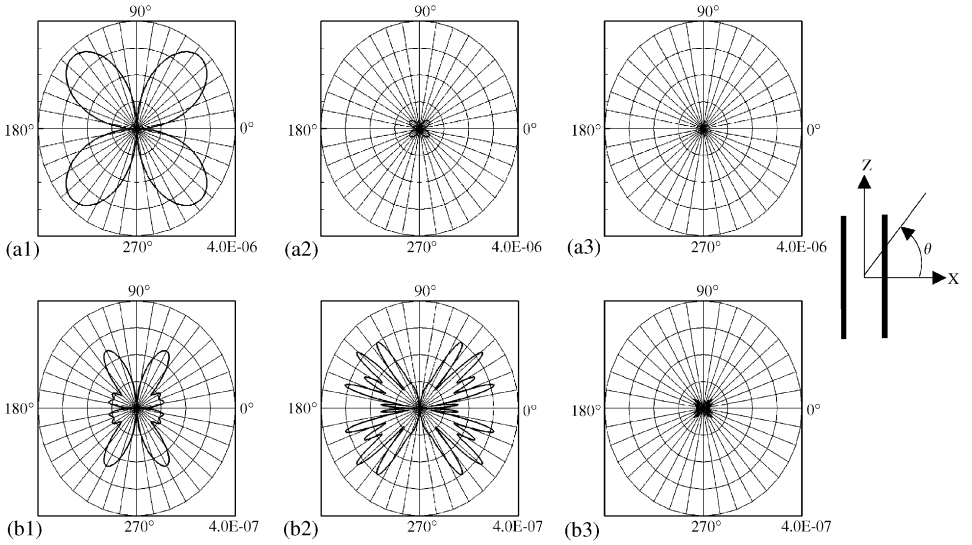


Fig. 14. Acoustic directivity patterns of a ducted rotating dipole source at $r = 7.5D_{\text{duct}}$, at $v^* = 0.0265\pi$ ((a1): free field—the 1st BPF, (a2): free field—the 2nd BPF, (a3): free field—the 3rd BPF, (b1): ducted field—the 1st BPF (cutoff), (b2): ducted field—the 2nd BPF (cuton), (b3): ducted field—the 3rd BPF (cuton), $v^* = D_s\Omega/2a_0$).

magnitude of (b1), (b2) and (b3). The magnitude of the harmonic frequency of the source decreases in a free field for the higher harmonics (see (a1), (a2) and (a3)). However, the magnitude of the harmonic frequency of the source in the duct shows different patterns (see (b1), (b2) and (b3)). It is interesting that the magnitude of the second BPF for the duct case is larger than that of the first BPF (see (b1) and (b2)). This is because the first BPF is cutoff and the second BPF is cuton.

## 4. Concluding remarks

A numerical method for calculating sound radiation from a rotating dipole source in an opened thin duct is developed. The Kirchhoff surface is introduced as a means to model the rotating source in the frequency domain to include the diffraction effect from the finite duct. When modeling the rotating source as the fixed distributed sources on the Kirchhoff surface, the acoustic pressure of the rotating source and the normal derivative of the pressure should be obtained. In this paper, the normal derivative of the acoustic pressure on the surface has been derived analytically. It has been shown that the acoustic pressure and the normal derivative of the acoustic pressure are well described through the Kirchhoff source on the thin duct wall. The K–H TBEM is well established and verified.

After verification of the K–H TBEM, the method was applied in the calculation of sound radiation from a ducted rotating dipole source. It was shown that sound radiation from the rotating source in the duct has different directivity patterns from those of the rotating source in a free field. Lower harmonics of the rotating source tend to be cutoff and higher harmonics tend to be cuton. Wave propagations of the rotating source are strongly dependent on the cutoff frequency of the duct circumferential modes.

## References

[1] M.V. Lowson, The sound field for singularities in motion, *Proceedings of Royal Society of London Series* A 286 (1965) 559–572.
[2] J.M. Tyler, T.G. Sofrin, Axial flow compressor noise studies, *Society of Automotive Engineers Transactions* 70 (1962) 309–332.
[3] W. Eversman, Radiated noise of ducted fans, DGLR/AIAA Paper No. 92-02-139, 1992.
[4] M. K. Myers, J. H. Lan, Sound radiation from ducted rotating sources in uniform motion, AIAA Paper No. 93-4429, 1993.
[5] M.H. Dunn, J. Tweed, F. Farassat, The Application of a boundary integral equation method to the prediction of ducted fan engine noise, *Journal of Sound and Vibration* 227 (1999) 1019–1048.

[6] W.H. Jeon, D.J. Lee, A numerical study on the flow and sound fields of centrifugal impeller located near a wedge, *Journal of Sound and Vibration* 266 (2003) 785–804.
[7] W. H. Jeon, D. J. Lee, An analysis of generation and radiation of sound for a centrifugal fan, in: Seventh ICSV, 2000, pp. 1235–1242.
[8] T.W. Wu, G.C. Wan, Numerical modeling of acoustic radiation and scattering by thin bodies using a Cauchy principle integral equation, *Journal of the Acoustical Society of America* 92 (1992) 2900–2906.
[9] K.D. Ih, D.J. Lee, Development of the direct boundary element method for thin bodies with general boundary conditions, *Journal of Sound and Vibration* 202 (1997) 361–373.
[10] R. Martinez, *Diffracting open-ended pipe treated as a lifting surface AIAA* 26 (1988) 396–404.